

Multiple Nodeless Superconducting Gaps in $(\text{Ba}_{0.6}\text{K}_{0.4})\text{Fe}_2\text{As}_2$ Superconductor from Angle-Resolved Photoemission Spectroscopy

Lin Zhao¹, Haiyun Liu¹, Wentao Zhang¹, Jianqiao Meng¹, Xiaowen Jia¹, Guodong Liu¹,
Xiaoli Dong¹, G. F. Chen², J. L. Luo², N. L. Wang², W. Lu¹, Guiling Wang³, Yong
Zhou³, Yong Zhu⁴, Xiaoyang Wang⁴, Zuyan Xu³, Chuangtian Chen⁴, and X. J. Zhou^{1,*}

¹*National Laboratory for Superconductivity,*

*Beijing National Laboratory for Condensed Matter Physics,
Institute of Physics, Chinese Academy of Sciences, Beijing 100190, China*

²*Beijing National Laboratory for Condensed Matter Physics,
Institute of Physics, Chinese Academy of Sciences, Beijing 100190, China*

³*Key Laboratory for Optics, Beijing National Laboratory for Condensed Matter Physics,
Institute of Physics, Chinese Academy of Sciences, Beijing 100190, China*

⁴*Technical Institute of Physics and Chemistry,
Chinese Academy of Sciences, Beijing 100190, China*

(Dated: July 13, 2008)

Abstract

High resolution angle-resolved photoemission measurements have been carried out to study the superconducting gap in the $(\text{Ba}_{0.6}\text{K}_{0.4})\text{Fe}_2\text{As}_2$ superconductor with $T_c=35$ K. Two hole-like Fermi surface sheets around the Γ point exhibit different superconducting gaps. The inner Fermi surface sheet shows larger (10~12 meV) and slightly momentum-dependent gap while the outer one has smaller (7~8 meV) and nearly isotropic gap. The lack of gap node in both Fermi surface sheets favors s-wave superconducting gap symmetry. Superconducting gap opening is also observed at the $M(\pi,\pi)$ point. The two Fermi surface spots near the M point are gapped below T_c but the gap persists above T_c . These rich and detailed superconducting gap information will provide key insights and constraints in understanding pairing mechanism in the iron-based superconductors.

The recent discovery of superconductivity in iron-based compounds[1, 2, 3, 4, 5, 6, 7, 8, 9, 10] has generated great interest because they represent second class of high temperature superconductors after the discovery of the first high temperature superconductivity in copper-based compounds[11]. It is important to find out whether the superconductivity mechanism in this new system is conventional, or parallel to that in cuprates, or is along a new route in realizing high temperature superconductivity. The iron-based compounds share the same Fe_2As_2 layers that are believed to be responsible for superconductivity[1, 2, 3, 4, 5, 6, 7, 8, 9, 10]. Band structure calculations indicate that the low energy bands are dominated by the Fe $3d$ orbitals forming multiple Fermi surface sheets, hole-like Fermi surface sheets around the $\Gamma(0,0)$ point and electron-like Fermi surface sheets around the $M(\pi,\pi)$ point[12, 13, 14]. Information of the superconducting gap, i.e., the energy to break the electron pairs (Cooper pairs) that induces superconductivity, is intimately related to the superconductivity mechanism. At issue are whether the superconducting order parameter on various Fermi surface sheets is the same and, furthermore, whether its symmetry on different Fermi surface sheets is conventional s-wave-like or exotic[15, 16, 17, 18, 19, 20, 21]. Recent angle-resolved photoemission (ARPES) measurements have observed multiple Fermi surface sheets in these iron-based compounds[22, 23, 24, 25]. ARPES is also a unique probe in directly measuring the gap size and its momentum dependence[26].

In this paper we report direct observation of the superconducting gap in an iron-based ($\text{Ba}_{0.6}\text{K}_{0.4}$) Fe_2As_2 superconductor from angle-resolved photoemission spectroscopy measurement. We have found that the superconducting gap in the iron-based superconductors is complex and unusual. Different superconducting gaps are observed on the two Fermi surface sheets near the Γ point. The inner Fermi surface sheet shows larger (10~12 meV) and slightly momentum-dependent gap while the outer one has smaller (7~8 meV) and nearly isotropic gap. The lack of gap node in both Fermi surface sheets favors s-wave superconducting symmetry. Superconducting gap opening also occurs at the $M(\pi,\pi)$ point. The two Fermi surface spots near the M point are gapped below T_c but it is found that the gap persists above T_c . These rich and detailed gap information will provide key insights and constraints in developing theories in understanding the superconductivity mechanism in the new iron-based superconductors.

High resolution angle-resolved photoemission measurements are carried out on our lab

system equipped with the Scienta R4000 electron energy analyzer with a wide-angle-mode of 30 degrees[27]. We use Helium I resonance line as the light source with a photon energy of $h\nu=21.218$ eV. The light on the sample is partially polarized with the electric field vector mainly in the plane of the sample surface (as shown in Fig. 1b). The energy resolution was set at 4 meV and the angular resolution is ~ 0.3 degree. The Fermi level is referenced by measuring on a clean gold that is electrically connected to the sample. The $(\text{Ba}_{1-x}\text{K}_x)\text{Fe}_2\text{As}_2$ ($x=0.40$) single crystals were grown using flux method [28] and the crystal measured has a sharp superconducting transition at $T_c=35$ K with a transition width less than 2 K (Fig. 1a). The crystal was cleaved *in situ* and measured in vacuum with a base pressure better than 6×10^{-11} Torr.

Fig. 1b shows Fermi surface mapping of the $(\text{Ba}_{0.6}\text{K}_{0.4})\text{Fe}_2\text{As}_2$ superconductor by measuring photoemission spectral weight distribution integrated with a small energy window near the Fermi level E_F . Two hole-like Fermi surface sheets can be clearly identified around the Γ point, shown as two circles in Fig. 1b. Near the $M(\pi,\pi)$ point, no obvious closed Fermi surface sheet is observed. Instead, there are two strong intensity spots labeled as S1 and S2, respectively, observed on the Γ -M line, with their locations nearly symmetrical with respect to the M point. The appearance of these two Fermi surface spots is similar to those observed in $(\text{Sr},\text{K})\text{Fe}_2\text{As}_2$ superconductor[25].

Fig. 1(c) and (d) show photoemission images measured below T_c (Fig. 1c) and above T_c (Fig. 1d) along a typical momentum cut on the $\Gamma(0,0)$ - $M(\pi,\pi)$ line near the Γ point (Cut 1 in Fig. 1b). Three Fermi crossings are clearly observed with A1 and A2 being equivalent that correspond to the Fermi momenta for the inner Fermi surface sheet FS1, while A3 corresponds to the Fermi momentum of the outer Fermi surface sheet FS2. The corresponding photoemission spectra (energy distribution curves, EDCs) are shown in Fig. 1g and 1h, respectively. Clear EDC peaks develop in the superconducting state near the Fermi crossings (Fig. 1g).

Fig. 1(e) and (f) show photoemission images measured below and above T_c , respectively, along the Cut 2 (Fig. 1b) on the $\Gamma(0,0)$ - $M(\pi,\pi)$ line near the M point. Two Fermi crossings (B1 and B2) are clearly observed which correspond to the two strong intensity spots S1 and S2, respectively, in Fig. 1b. We note that, in the normal state, the band at the M point (Fig. 1f) appears to be above the Fermi level (Fig. 1i), as seen more clearly from the photoemission spectra at the M point which has a leading edge slightly above the Fermi

level E_F (Fig. 1j). This is consistent with the absence of enclosed electron-like Fermi surface sheets near the M point that are expected in the parent compound BaFe_2As_2 from the band calculations[14]. The introduction of holes in $(\text{Ba}_{0.6}\text{K}_{0.4})\text{Fe}_2\text{As}_2$ by doping potassium (K^+) into the barium (Ba^{2+}) site has lifted the related electron-like bands around the M point in BaFe_2As_2 slightly above the Fermi level. Interestingly, upon entering the superconducting state, a well-defined band develops below E_F (Fig. 1e) accompanied by appearance of sharp EDC peaks (Fig. 1i).

The identification of Fermi surface and the photoemission measurements above and below T_c make it possible to investigate the superconducting gap in this new superconductor. We start by first examining the superconducting gap near the Γ point. Fig. 2a shows the photoemission spectra on the two hole-like Fermi surface sheets above T_c and below T_c . To visually inspect possible gap opening and remove the effect of Fermi distribution function near the Fermi level, we have symmetrized the original EDCs to get spectra in Fig. 2(b-d) for the Fermi crossings A3, A2, and A1, respectively, following the procedure that is commonly used in high temperature cuprate superconductors[29]. The gap size is extracted from the peak position of the symmetrized EDCs. For the Fermi crossing A1 on the inner Fermi surface sheet FS1 (Fig. 2d), there is no gap opening above T_c , while a clear superconducting gap opens at 14 K with a size of ~ 10 meV. The situation on another equivalent crossing A2 is similar to A1 (Fig. 2c). For the Fermi crossing A3 on the outer Fermi surface sheet FS2, one can also see superconducting gap opening, but with a gap size slightly smaller, ~ 8 meV, as seen from Fig. 2b.

The observation of two hole-like Fermi surface sheets around the Γ point (Fig. 1b) provides a good opportunity to investigate the momentum dependence of the superconducting gap that is crucial in determining the gap symmetry. Fig. 3a and 3b show photoemission spectra around the two Fermi surface sheets FS2 and FS1 near Γ , respectively, measured in the superconducting state ($T=14$ K). The corresponding symmetrized spectra are shown in Fig. 3c and 3d. The extracted superconducting gaps on both Fermi surface sheets are plotted in Fig. 3e. The superconducting gap on the outer Fermi surface sheet FS2 are nearly constant around the Fermi surface with a size of ~ 8 meV. For the inner Fermi surface sheet FS1, there is a slight variation of the superconducting gap with momentum: it is largest along the Γ -X and Γ -Y directions (~ 12 meV) and smallest along the Γ -M direction (~ 10 meV).

Now let us check on the superconducting gap near the M point. Fig. 4 shows photoemission spectra at the two Fermi spots S1 (Fig. 4a) and S2 (Fig. 4c), as well as at the M point (Fig. 4b) measured at different temperatures. For the two equivalent Fermi crossings S1 and S2, it is clear that there is a gap in the superconducting state with a size of ~ 11 meV. However, upon entering the normal state above T_c , the gap persists at both locations with a gap size unchanged or even getting slightly larger. This behavior is similar to that observed in high temperature cuprate superconductors where near the $(\pi,0)$ point in the underdoped samples, a gap opening is observed above T_c which is associated with the opening of a pseudogap[26].

It is interesting to see that at the M point there is a clear signature of the superconducting gap opening below T_c . As mentioned before and seen from Figs. 1f and 1j, above T_c , the band at the M point is slightly above the Fermi level. However, upon entering the superconducting state, the photoemission spectra pull back to below the Fermi level, forming a well-defined band (Fig. 1e) with sharp EDC peaks (Fig. 1i and 4b). From Fig. 4e, it is clear that above T_c there is no gap, but below T_c there is a superconducting gap opening with a size of 10 meV at 14 K. It gets smaller with increasing temperature and becomes 7 meV at 25 K, and vanishes at and above T_c (Fig. 4g).

From the above observations, it becomes clear that the superconducting gap in the iron-based $(\text{Ba}_{0.6}\text{K}_{0.4})\text{Fe}_2\text{As}_2$ superconductor is complex and unusual. (1). Superconducting gap is different on different Fermi surface sheets, as evidenced from the gap on the two hole-like Fermi surface sheets around the Γ point (Fig. 3). This has established a clear case that the iron-based superconductors have multiple gaps like the well-established case of MgB_2 [30]. (2). For the inner hole-like Fermi surface sheet FS1 near the Γ point, it shows a slightly anisotropic superconducting gap with a size of $\Delta_{FS1}=10\sim 12$ meV. This gives a ratio of $2\Delta_{FS1}/kT_c=6.9\sim 8.2$ which is significantly larger than the traditional BCS weak-coupling value of 3.52. For the outer sheet FS2 near the Γ point, it shows a smaller and nearly isotropic superconducting gap with a size of $\Delta_{FS2}=7\sim 8$ meV. This gives $2\Delta_{FS2}/kT_c=4.8\sim 5.5$ which is still larger than the traditional BCS value. Both cases have put the iron-based superconductors in the strong coupling regime. (3). Although ARPES measures the gap amplitude but not the phase of the superconducting order parameter, the lack of gap nodes on both Fermi surface sheets around the Γ point favors s-wave superconducting gap symmetry. These will put strong constraints on various gap symmetries and the underlying pairing mechanisms

proposed for the iron-based superconductor[15, 16, 17, 18, 19, 20, 21]. (4). For the two Fermi spots S1 and S2 near the M point, they show a gap below T_c but the gap persists above T_c (Fig. 4). (5). It is interesting that the M point shows clear superconducting gap opening although in the normal state the band is slightly above the Fermi level. These rich and detailed information will provide key insights in developing theories for understanding superconductivity mechanism of the iron-based superconductors.

We thank T. Xiang for useful discussions. This work is supported by the NSFC, the MOST of China (973 project No: 2006CB601002, 2006CB921302), and CAS (Projects IT-SNEM).

*Corresponding author: XJZhou@aphy.iphy.ac.cn

-
- [1] Y. Kamihara et al., *J. Am. Chem. Soc.* **130**, 3296 (2008).
 - [2] X. H. Chen et al., *Nature (London)* **453**, 761 (2008).
 - [3] G. F. Chen et al., *Phys. Rev. Lett.* **100**, 247002 (2008).
 - [4] Z. A. Ren et al., *Europhys. Lett.* **82**, 57002 (2008).
 - [5] Z. A. Ren et al., arXiv:cod-mat/0803.4283.
 - [6] Z. A. Ren et al., *Chin. Phys. Lett.* **25**, 2215 (2008).
 - [7] M. Rotter et al., arXiv:cod-mat/0805.4630.
 - [8] K. Sasmal et al., arXiv:cod-mat/0806.1301.
 - [9] G. F. Chen et al., arXiv:cod-mat/0806.1209.
 - [10] G. Wu et al., arXiv:cod-mat/0806.1459.
 - [11] J. G. Bednorz and K. A. Mueller, *Z. Phys. B* **64**, 189 (1986).
 - [12] J. Dong et al., *Europhys. Lett.* **83**, 27006 (2008).
 - [13] D. J. Singh and M.-H. Du, *Phys. Rev. Lett.* **100**, 237003 (2008).
 - [14] I. A. Nekrasov et al., arXiv:cod-mat/0806.2630.
 - [15] I. I. Mazin et al., arXiv:cod-mat/0803.2740.
 - [16] K. Kuroki et al., arXiv:cod-mat/0803.3325.
 - [17] X. Dai et al., arXiv:cod-mat/0803.3982.
 - [18] P. A. Lee et al., arXiv:cod-mat/0804.1739.
 - [19] Z. J. Yao et al., arXiv:cod-mat/0804.4166.

- [20] K. Seo et al., arXiv:cod-mat/0805.2958.
- [21] F. Wang et al., arXiv:cod-mat/0805.3343.
- [22] C. Liu et al., arXiv:cond-mat/0806.2147.
- [23] L. X. Yang et al., arXiv:cond-mat/0806.2627.
- [24] C. Liu et al., arXiv:cond-mat/0806.3453.
- [25] H. Y. Liu et al., arXiv:cod-mat/0806.4806.
- [26] A. Damascelli et al., Rev. Mod. Phys. **75**, 473 (2003).
- [27] G. D. Liu et al., Rev. Sci. Instruments **79**, 023105 (2008).
- [28] G. F. Chen et al., arXiv:cod-mat/0806.2648.
- [29] M. R. Norman et al., Phys. Rev. B **57**, R11093 (1998).
- [30] H. J. Choi et al., Nature (London) **418**, 758 (2002).

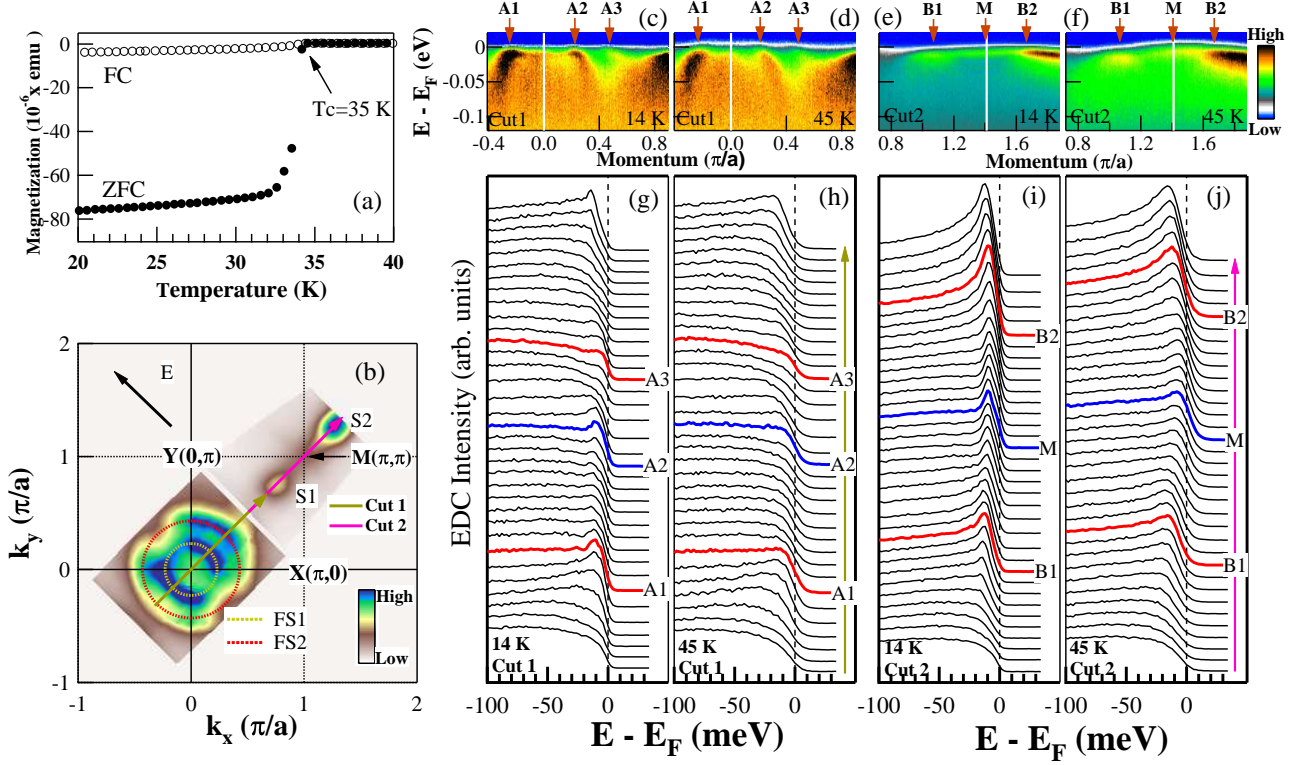


FIG. 1: Fermi surface, band structure and photoemission spectra of $(\text{Ba}_{0.6}\text{K}_{0.4})\text{Fe}_2\text{As}_2$ superconductor ($T_c=35 \text{ K}$). (a). Magnetic measurement of T_c for the $(\text{Ba}_{0.6}\text{K}_{0.4})\text{Fe}_2\text{As}_2$ single crystal. The onset T_c is 35 K with a sharp transition width of $\sim 1.5 \text{ K}$. (b). Spectral weight distribution integrated within $[-5\text{meV}, 5\text{meV}]$ energy window with respect to the Fermi level as a function of k_x and k_y measured at 14 K. The black arrow near the up-left marks the main electric field direction on the sample surface from the light source. The two hole-like Fermi surface sheets observed around Γ point are shown as two circles marked as FS1 for the inner sheet and FS2 for the outer one. Near the $M(\pi, \pi)$ point along the $\Gamma(0,0)$ - $M(\pi, \pi)$ direction, two strong intensity spots are observed and labeled as S1 and S2, respectively. (c) and (d) show photoemission images measured along the Cut 1 at 14 K and 45 K, respectively, while (e) and (f) show photoemission images along the Cut 2 at 14 K and 45 K, respectively. The locations of the Cuts 1 and 2 are marked in Fig. 1b. (g-j) show corresponding photoemission spectra at 14 K and 45 K along the two cuts, with photoemission spectra at the Fermi momenta colored and marked.

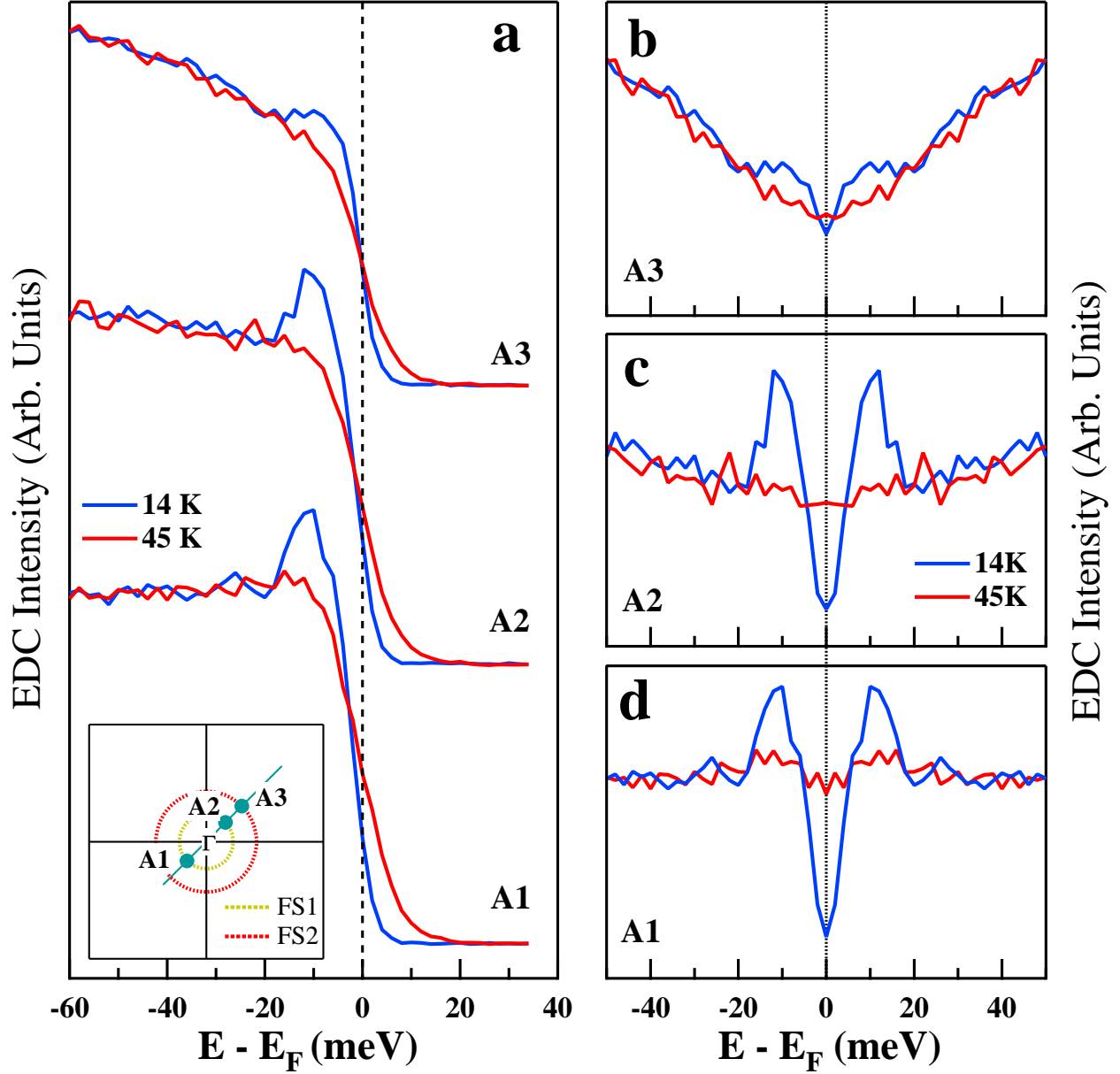


FIG. 2: Superconducting gap near the Γ point. (a). Photoemission spectra above and below T_c at three Fermi crossings (A1, A2 and A3) on the two hole-like Fermi surface sheets shown in the bottom-left inset. (b), (c) and (d) show symmetrized photoemission spectra for the Fermi crossings A3, A2 and A1, respectively.

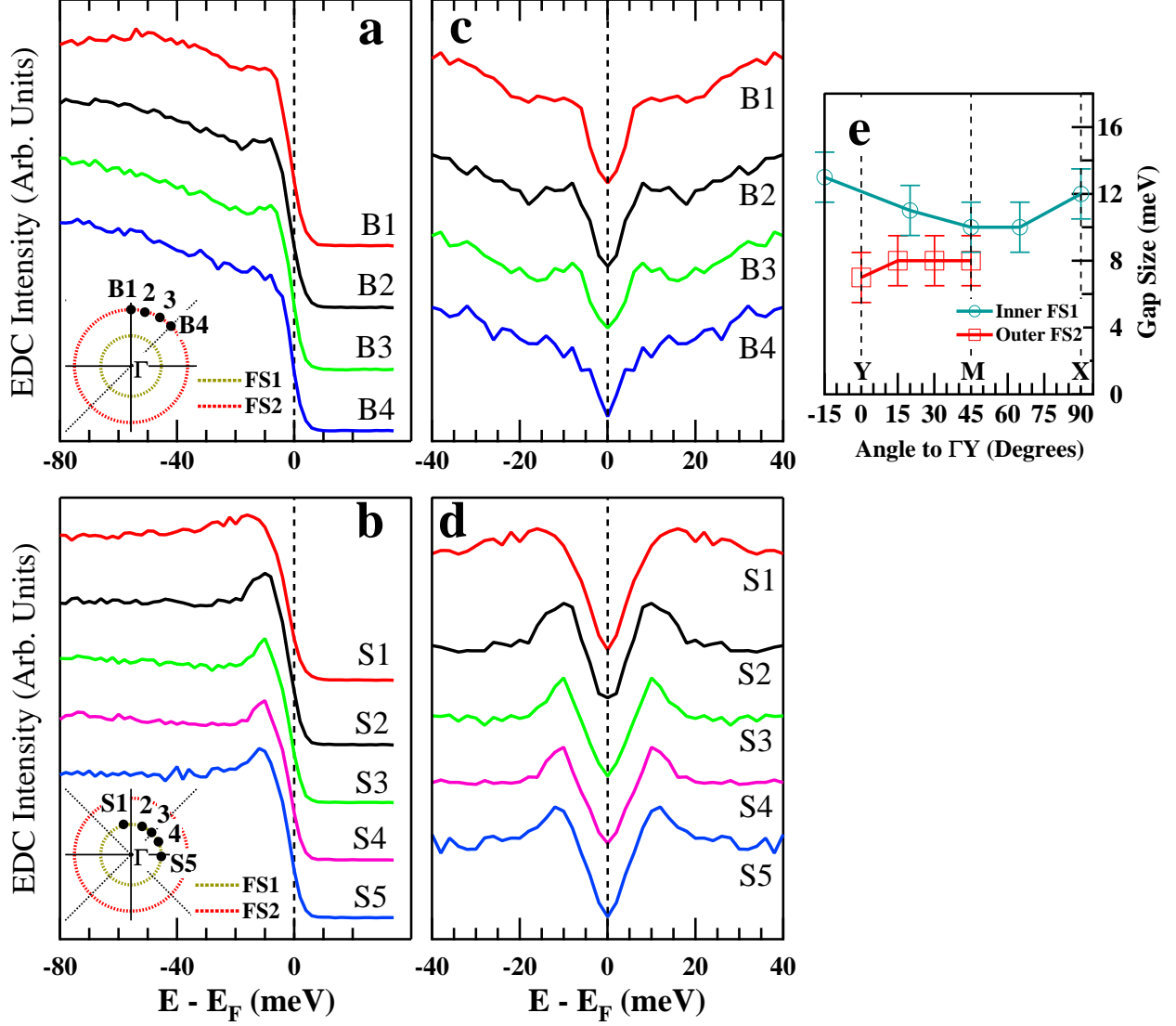


FIG. 3: Momentum dependent photoemission spectra and superconducting gap measured at $T=14$ K. (a) and (b) show photoemission spectra on the outer Fermi surface FS2 and inner Fermi surface sheet FS1, respectively. (c) and (d) show corresponding symmetrized photoemission spectra. (e). Momentum dependent superconducting gap as a function of angle for the two Fermi surface sheets. The angle is defined with respect to the $\Gamma(0,0)$ - $Y(0,\pi)$ line.

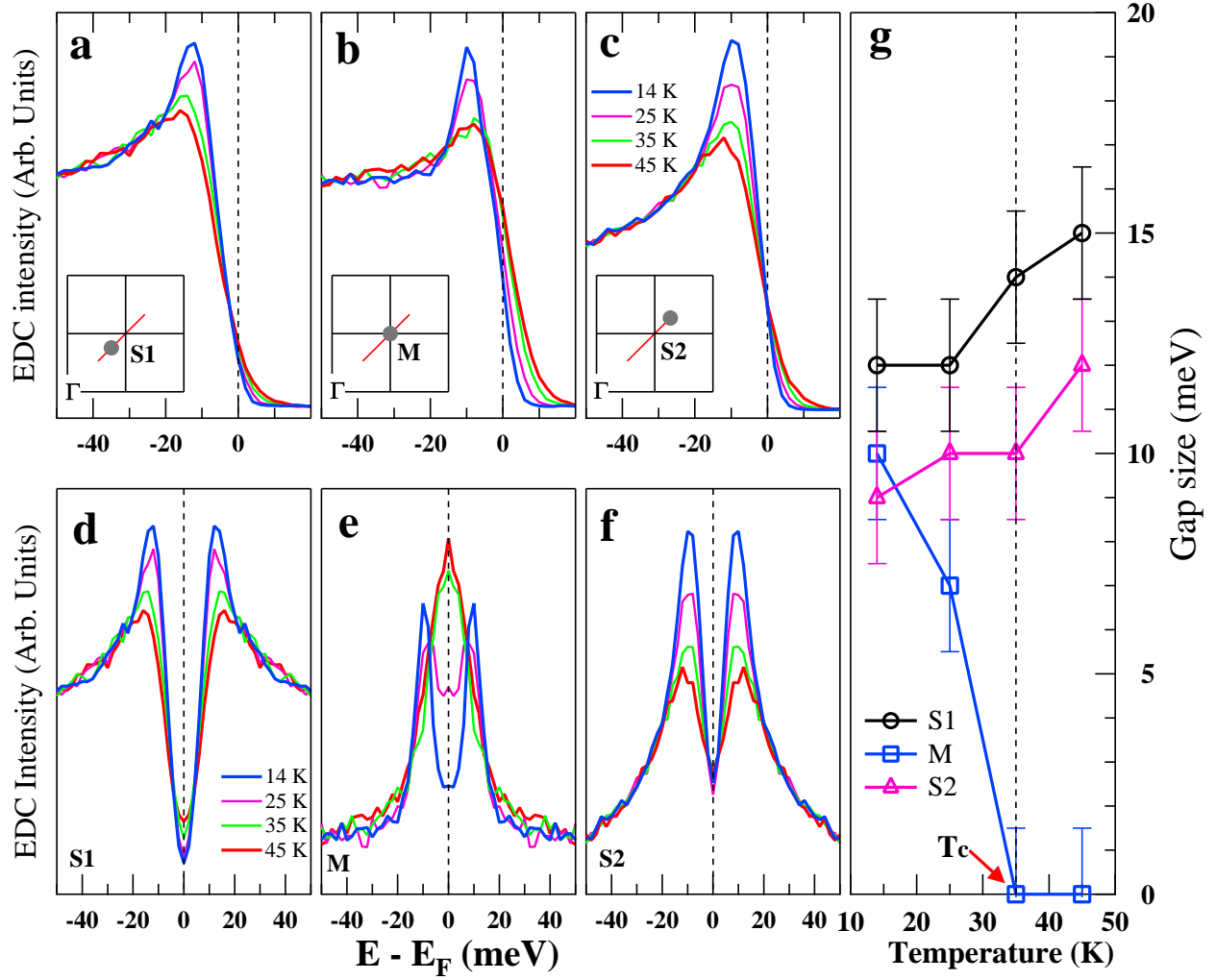


FIG. 4: Superconducting gap near the $M(\pi, \pi)$ point. (a), (b) and (c) show photoemission spectra measured at S1, M and S2 points at different temperatures. (d), (e) and (f) show corresponding symmetrized photoemission spectra. (g) plots the gap size extracted for the S1, M and S2 points as a function of temperature.